Structure and dynamics of surfactant-stabilized aggregates of palladium nanoparticles under dilute and semidilute conditions: Static and dynamic x-ray scattering

T. Thurn-Albrecht,* G. Meier, P. Müller-Buschbaum, A. Patkowski,† and W. Steffen
Max-Planck-Institut für Polymerforschung, Ackermannweg 10, 55128 Mainz, Germany

G. Grübel, D. L. Abernathy, and O. Diat
European Synchrotron Radiation Facility, Boîte Postale 220, 38043 Grenoble, France

M. Winter, M. G. Koch, and M. T. Reetz
Max-Planck-Institut für Kohlenforschung, Kaiser-Wilhelm-Platz 1, 45470 Mülheim/Ruhr, Germany
(Received 28 July 1998)

We have used high-resolution small-angle x-ray scattering and the recently introduced technique of x-ray photon correlation spectroscopy to study the structure and diffusive dynamics of a colloidal palladium aggregate sol under dilute and semidilute conditions. At low concentration we find that the size of the aggregates as determined from the static structure factor and from the diffusive dynamics agree. At high concentration the aggregates start to overlap and the apparent diffusion constant decreases, while the system remains in a liquidlike state. The comparison of static and dynamic data gives insight into structural features that are indiscernable by one technique alone. [S1063-651X(99)00701-1]

PACS number(s): 82.70.Dd, 61.10.Eq, 61.43.Hv, 61.46.+w

I. INTRODUCTION

The irregularly shaped objects formed during aggregation processes are scale invariant and can be described by the concepts of fractal geometry. This was shown by computer modeling [1–5] and later confirmed by experiments [6–8]. Recently the interest in aggregate sols has turned to the investigation of more concentrated systems, stimulated by the observation that in these systems a preferred length scale can exist [9–11]. Due to their open, fractal structure, aggregates in solutions can build up space filling structures at very modest volume fractions. The dynamics of such a concentrated system could in one case successfully be described in terms of internal modes of a gel with arrested translational and rotational diffusion [12], but simultaneous studies of the structure and the dynamics of these systems remain sparce.

In this paper we present a study of the structure and the dynamics of a surfactant-stabilized aggregate sol using static and dynamic x-ray scattering. Concentrations up to the semidilute regime, in which the size of the aggregate is comparable to the distance between aggregates, are covered. The aggregates consist of colloidal palladium particles with a size of a few nanometers. Transition metal particles in the size range 1–10 nm have attracted considerable interest due to their potential use in catalysis. The behavior of water-based sols such as the one under study are therefore of particular interest.

For our study we combined high-resolution small-angle x-ray scattering (SAXS) with x-ray photon correlation spectroscopy (XPCS). This recently introduced technique allows the investigation of the dynamics of concentrated, structured systems at high scattering vectors [13,14]. Interesting features of the SAXS data are illuminated by combining the results of static and dynamic experiments.

II. SCATTERING EXPERIMENTS ON COLLOIDAL AGGREGATE SOLUTIONS

A. Static scattering cross section

The x-ray scattering cross section for a system of identical particles is

$$\frac{d\sigma}{d\Omega} = r_e^2 V I(q). \tag{1}$$

Here r_e^2 is the Thompson scattering cross section of a single electron and V is the scattering volume. The scattering intensity $I(q)$ is given by

$$I(q) = \frac{1}{r_e^2 V}\frac{d\sigma}{d\Omega} = c_p v_p^2 \Delta\rho_e^2 |F(q)|^2 S(q) \quad \text{(eu/volume)}, \tag{2}$$

where c_p denotes the number concentration of particles, v_p is the volume of the particles, and $\Delta\rho_e$ is the electron density difference between the particles and the surrounding medium. $F(q)$ is the form factor of the individual particles and the structure factor $S(q)$ gives the effect of interparticle correlations. Although the exact expression for $F(q)$ depends on the shape and size of the particles, generally valid asymptotic formulas for small and large q values can be given [15]. For small q the Guinier approximation is valid, so that

$$|F(q)|^2 = \exp(-q^2 R_g^2/3) \quad \text{for} \quad qR_g \lesssim 1. \tag{3}$$

*Present address: Department of Polymer Science and Engineering, University of Massachusetts Amherst, MA 01003.

†Also at the Institute of Physics, A. Mickiewicz University, Poznan, Poland.

Here R_g is the Guinier radius of the particles. For large q the q dependence is given by Porod's law

$$|F(q)|^2 \sim q^{-4} \quad \text{for } qR_g \gg 1. \tag{4}$$

The structure factor of the system is given by

$$S(\vec{q}) = \frac{1}{N} \sum_{i,j} \exp[-i\vec{q}\cdot(\vec{R}_i - \vec{R}_j)]. \tag{5}$$

The sum $\Sigma_{i,j}$ in Eq. (5) extends over all N particles at the positions $\vec{R}_i$ in the sample. $S(\vec{q})$ is related to the particle pair correlation function $c(\vec{r})$ by

$$S(\vec{q}) = \int \exp(-i\vec{q}\cdot\vec{r})[c(\vec{r}) - \langle c\rangle] d^3r. \tag{6}$$

The correlation function $c(\vec{r})$ is composed of a δ function describing the self-correlation part and a contribution $c'(\vec{r})$ taking into account correlations between different particles,

$$c(\vec{r}) = \delta(\vec{r}) + c'(\vec{r}). \tag{7}$$

In an isotropic system $S(\vec{q})$ and $c(\vec{r})$ depend only on the moduli $|\vec{q}|$ and $|\vec{r}|$ and Eq. (6) simplifies to

$$S(q) = 4\pi \int_0^\infty \frac{\sin qr}{qr} [c(r) - \langle c\rangle] r^2 dr. \tag{8}$$

For a dilute solution of particles only the self-correlation part contributes and $S(q) = 1$. This is generally the limiting value of $S(q)$ for $q \to \infty$ in a system without long-range order. In the case where the particles form aggregates consisting of n_{agg} particles and interferences are limited to within one aggregate, $S(q) = n_{agg}$ for $q \to 0$. Using Eq. (2) and noting that $F(q \to 0) = 1$, the scattering intensity as q goes to zero for a dilute aggregated system is

$$I(q \to 0)_{dilute} = c_p v_p^2 \Delta\rho_e^2 n_{agg} = c_{agg} v_{agg}^2 \Delta\rho_e^2. \tag{9}$$

Here c_{agg} is the number concentration of aggregates and v_{agg} the volume of an aggregate. Again a Guinier approximation as in Eq. (3) can be used for small q and

$$I(q) = I(0)\exp(-q^2 R_{g,agg}^2/3) \quad \text{for } qR_{g,agg} \lesssim 1. \tag{10}$$

$R_{g,agg}$ is now the Guinier radius of the aggregates.

Beyond the Guinier range the shape of $S(q)$ reflects the internal structure of the aggregates. This is most easily described in terms of the correlation function $c(r)$. A useful form is given by

$$c(r) \propto r^{d_f - 3} f(r/R). \tag{11}$$

The power law r^{d_f-3} describes the scaling typical for a fractal of dimension d_f and leads to an asymptotic power law in the scattering curve $S(q) \sim q^{-d_f}$. $f(r/R)$ is a cutoff function taking into account that the structure can only be described as fractal up to a length R. Thus

$$S(q) \propto \int_{r_0}^\infty r^{d_f - 3} f(r/R) \frac{\sin(qr)}{qr} r^2 dr, \tag{12}$$

where r_0 is of the order of the size of the constituting particles of the aggregates. Choosing a simple cutoff function $f(r/R) = \exp(-r/R)$, the integral (12) can be solved analytically if $r_0 \ll R$ [16] and

$$S(q) \propto \frac{1}{(qr_0)^{d_f}} \frac{d_f \Gamma(d_f - 1)}{(1 + 1/q^2R^2)^{(d_f-1)/2}} \sin[(d_f - 1)\arctan(qR)]. \tag{13}$$

Here Γ denotes the gamma-function. The expression (13) may be used to describe the finite size of isolated aggregates, but was originally devised to describe overlapping aggregates in a dense system, a situation that has been realized in dry powders of aggregating particles [8,17]. Expanding equation (13) for small q leads to

$$S(q) \approx S(0)[1 - q^2 d_f (d_f + 1) R^2/6]. \tag{14}$$

If the solution becomes more concentrated interferences between different aggregates cannot be neglected any longer, especially around $q = 0$. The value of $S(q \to 0)$ is then not related in any simple way to the number of particles in the system. Nevertheless, a correlation length ξ can be extracted from the shape of the structure factor in this region by taking

$$\left.\frac{d^2S}{dq^2}\right|_{q=0} = -2\xi^2 S(0). \tag{15}$$

This is equivalent to an Ornstein-Zernicke approximation for $S(q)$ usually written as

$$S(q) \approx \frac{S(0)}{1 + q^2\xi^2}. \tag{16}$$

Note that this behavior is up to order q^2 indistinguishable from the Guinier expression (10), which is only meaningful for a dilute solution.

B. Photon correlation spectroscopy with coherent x rays

Photon correlation spectroscopy using visible light is a widely used scattering technique to study low-frequency dynamics in disordered systems [18,19]. Since it requires the use of highly coherent radiation, it became available for x rays only recently with the advent of third-generation synchrotron radiation sources. This technique probes the dynamic properties of matter by measuring the temporal correlation of the intensity scattered by the sample. Correlations are quantified via the normalized time correlation function $g(t)$:

$$g(t) = \frac{\langle n(t')n(t'+t)\rangle}{\langle n\rangle^2}, \tag{17}$$

where $n(t)$ is the number of photons scattered in an interval Δt around a time t,

$$n(t) = \int_{\Delta t} I(t) dt. \tag{18}$$

The angular brackets in Eq. (17) denote the time average. The intensity correlation function (17) is related to the field correlation function, which resembles the intermediate scattering function in terms of which inelastic scattering experiments are usually described:

$$\frac{\langle I(q,0)I(q,t)\rangle}{\langle I(q)\rangle^2}=1+\beta\frac{\langle E(q,0)E^*(q,t)\rangle^2}{\langle I(q)\rangle^2}. \qquad (19)$$

β is a constant that under fully coherent conditions would be equal to unity. Depending on the amount of incoherent averaging introduced by the partial coherence of the beam and the geometrical details of the experimental setup, it can take values between zero and one (Appendix A).

For a translational diffusion process the expected functional form of the correlation function $g(t)$ is [18]

$$g(q,t)=A(q)e^{-2\Gamma_q t}+1 \quad \text{with} \quad \Gamma=q^2D. \qquad (20)$$

D is a diffusion coefficient. For translational diffusion under dilute conditions one expects

$$D(c\rightarrow 0)=D_0=\frac{kT}{6\pi\eta R_h}. \qquad (21)$$

Here k is the Boltzmann constant, T the temperature, η the viscosity of the solvent, and R_h the hydrodynamic radius of the diffusing particles. If the solution is more concentrated particles will interact and interparticle interferences come into play. Then the measured $D(q)$ is an effective diffusion coefficient and reflects more generally the relaxation rate of concentration fluctuations with wave vector q. In the limit of high q this effective diffusion coefficient D reduces to the short-time self-diffusion coefficient D_s [20]. Without a hydrodynamic interaction D_s is identical to the diffusion constant D_0 given in Eq. (21), but generally D_s will be somewhat reduced in comparison to D_0 [20].

III. EXPERIMENTAL DETAILS

A. Ultrasmall-angle x-ray scattering

The measurements were taken at the European Synchrotron Radiation Facility (ESRF) on beam line 2 using a Bonse-Hart setup with two crossed channel cut monochromators for the incoming and the scattered beam effectively producing point collimation. The smallest accessible scattering vector ($q_{min}\sim 6\times 10^{-4}$ Å^{-1}) is the q at which the background caused by diffuse scattering from the crystals and absorbers is comparable in intensity to the scattering signal from the sample. X rays with an energy of 12.4 keV ($\lambda=1$Å) were used. The experimental setup is described in detail in [21]. Measurements of the static structure factor covering the q range from 0.01 to 0.5 Å^{-1} were taken with a Kratky camera mounted on a conventional sealed x-ray tube. This setup uses slit collimation, which requires deconvolution of the measured data [22]. The primary beam intensity is measured with a moving slit, which allows the determination of absolute values of scattering cross sections.

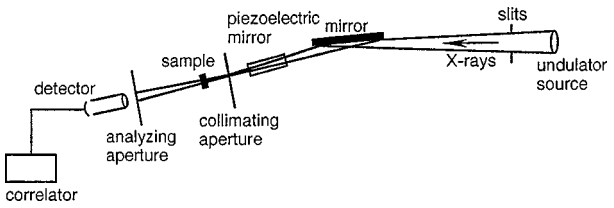

FIG. 1. Schematic setup of the Troika beam line for the experiment.

B. X-ray photon correlation spectroscopy

For a coherent scattering experiment the scattering volume has to be adjusted to the coherence lengths of the radiation used. Whereas this requirement is relatively easy to fulfill with laser light, it requires a highly collimated beam in the case of x rays that can be produced only by using very small (micrometer-sized) pinholes. The experiment was performed on beam line 9 (TROIKA) at the ESRF. The beam line was configured to provide maximum coherent flux by restricting the longitudinal coherence length ξ_l to about 100 Å. The transverse coherence length ξ_t amounted to about 15 μm and a pinhole of that size was used to produce a nominally coherent beam. Figure 1 shows a schematic layout of the setup. The setup and the coherence properties of the beam are described in detail in [23]. The undulator source was tuned to an energy of 8.1 keV ($\lambda=1.53$ Å). Correlation functions were measured by a digital ALV5000/E (ALV Langen, Germany) correlator.

IV. SAMPLES

The colloidal particles under study are synthesized via an electrochemical method recently introduced by Reetz and coworkers [24,25]. The synthesis proceeds via electrochemical reduction of metal ions in the presence of a stabilizing agent. Which type of stabilizer is to be used depends on the solvent. Water soluble metal colloids (hydrosols) can be obtained using zwitterionic surfactants of the sulfobetaine type [26,27]. For the sample studied dimethyldodecylammoniopropanesulfonate ($C_{12}H_{25}[CH_3]_2N^+C_3H_6SO_3^-$) was used as a stabilizer. TEM gave a radius of 20–30 Å for the metallic particles. The dry powder has a metal weight content of 26.8% and is easily dispersed in water. On dilution the colloidal solution becomes unstable in the concentration range in which the surfactant content falls below the critical micelle concentration (2 mmol/l [28]). In the concentration range under study no sedimentation was observed. A thin glass capillary with a diameter of 1 mm served as the sample container.

V. RESULTS

A. Statics

Figure 2 shows the static scattering cross section $I(q)$ of three solutions with different concentrations of a palladium colloid. The palladium volume fractions Φ_{Pd} as calculated from the weight fractions are 6.4×10^{-4} (sample 1), 2.3×10^{-3} (sample 2), and 7.9×10^{-3} (sample 3), with the highest concentration showing the most intense scattering. The curves can be split into several q regimes reflecting struc-

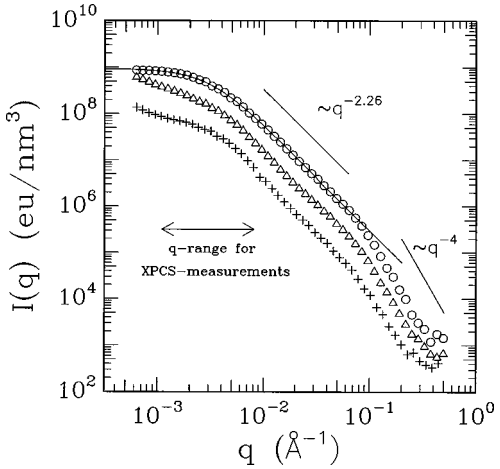

FIG. 2. Scattering cross section $I(q)$ vs q of the Pd colloid in water at three different volume fractions: $\phi=6.4\times10^{-4}$, + (sample 1), $\phi=2.3\times10^{-3}$, △, (sample 2), and $\phi=7.9\times10^{-3}$, ○ (sample 3). The solid line is a fit of the model function (13) to the data obtained from sample 3.

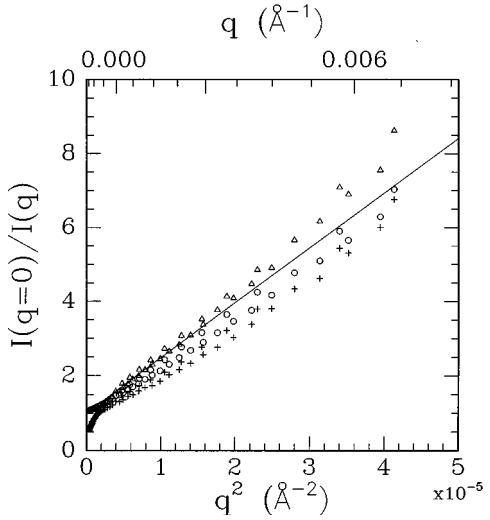

FIG. 3. Scattering cross section $I(q)$ as in Fig. 2 in a representation linearizing the Ornstein-Zernicke expression (16). All three curves show a similar slope reflecting a similar correlation length. The solid line corresponds to a correlation length $\xi=385$ Å. Deviations from the linear behavior in samples 1 and 2 at very small q are disregarded here. +, $\phi=6.4\times10^{-4}$ (sample 1); △, $\phi=2.3\times10^{-3}$ (sample 2); and ○, $\phi=7.9\times10^{-3}$ (sample 3).

tures on different scales. Starting on the high q side, the smallest structural unit, i.e., the individual Pd particles, determines the shape of $I(q)$. In agreement with the TEM results, the scattering cross section displays Porod behavior, i.e., $I(q)\propto q^{-4}$, beyond $q\sim0.1$ Å^{-1}. At lower scattering vectors ($q\lesssim0.1$ Å^{-1}) an additional increase of $I(q)$ is observed, indicating the existence of aggregates whose internal structure is reflected in this q range. Here $I(q)$ follows approximately a power law $I(q)\propto q^{-d_f}$, d_f being the fractal dimension of the aggregate. Below about 6×10^{-3} Å^{-1} the structure factor of all three samples deviates from the power law, which indicates the finite extension of the fractal structure. Using the quadratic approximation (16) to describe $I(q)$ in this range, a correlation length ξ can be extracted. Figure 3 shows the data in a representation that linearizes Eq. (16). Up to deviations of about 10%, samples 1, 2, and 3 are characterized by the same correlation length of 385 Å.

Inspection of Fig. 2 shows that all three data sets are basically parallel, indicating a structure independent of concentration. Only at the lowest q values ($q\lesssim2\times10^{-3}$ Å^{-1}) are there differences in the slope of the curves. The sample with the highest concentration (open circles) displays the most simple shape of the scattering curve. It can very well be described by the expression (13) introduced above as a model for a fractal structure with finite extent. The corresponding model curve is shown in Fig. 2. The fractal dimension determined from the fit is $d_f=2.26\pm0.05$. $I(0)$ is 9.3×10^8 eu/nm^3 and the value of R is 308 ± 5 Å. Comparing Eqs. (14) and (15), this corresponds to a correlation length ξ of 341 Å. This is in accordance with our previous result based on Eq. (16). A fit of Eq. (13) to the more dilute samples does not lead to a satisfatory description. This point is dicussed in detail below.

The description of the SAXS data thus far does not reveal the state of dilution of the solution. A simple estimate shows that the data obtained from sample 3 ($\Phi_{\mathrm{Pd}}=7.9\times10^{-3}$) are not consistent with the assumption of a dilute solution. Assuming for a moment a dilute solution, we may employ Eq. (9). c_{agg} and v_{agg} are related to the Pd volume fraction ϕ,

$$\phi=c_{agg}v_{agg}. \tag{22}$$

ϕ can be calculated from the known weight fraction of palladium. Combining Eqs. (9) and (22), we get an expression for c_{agg},

$$c_{agg}=\frac{\Delta\rho_e^2\phi^2}{I(0)}. \tag{23}$$

Here the scattering by the surfactant in the solution can be neglected since the electron density of palladium as compared to organic material is about a factor of 10 higher (H_2O, $\rho_e=335$ nm^{-3}; Pd, $\rho_e=3124$ nm^{-3}). From c_{agg} a typical distance d between aggregates in the solution can be estimated, $d\approx c_{agg}^{-1/3}$. With $I(0)=9.3\times10^8$ eu/nm^3, we obtain $c_{agg}=5.2\times^{-7}$ nm^{-3} and $d\approx1240$ Å. On the other hand, in a dilute solution the correlation length determined above can be interpreted in terms of the Guinier approximation (10), i.e., $R_{g,agg}=\sqrt{3}\xi=667$ Å$\pm10\%$. This means that the estimated distance between aggregates is comparable to the diameter $2R_{g,agg}$ of the aggregates. We conclude that at least for sample 3 with the highest concentration we reached a semidilute state in which the aggregates partially overlap.

We now proceed with the analysis of the mentioned differences in the structure factors in the range $q\lesssim2\times10^{-3}$ Å^{-1}. The scattering curve measured on the more dilute samples 1 and 2 shows an additional longer correlation length. By plotting $I(q\to0)/I(q)$ versus q^2 for the range of the smallest q, the value of this large correlation length can be determined according to Eq. (16). The result is shown in Fig. 4. The values of 1421 Å (sample 1) and 1119 Å (sample 2) are about a factor 3–4 greater than the smaller correlation length dominating the structure factor of sample 3 and also present in samples 1 and 2. A precise interpreta-

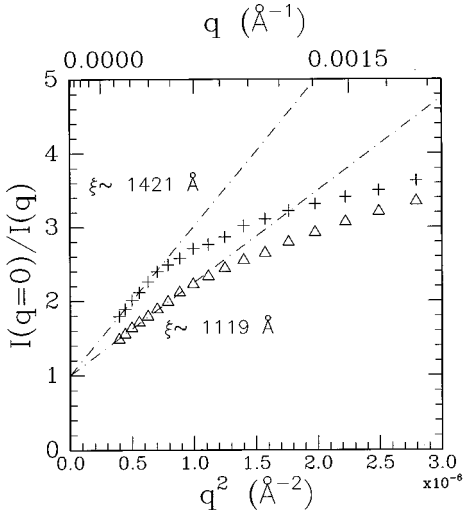

FIG. 4. Scattering cross section $I(q)$ as in Fig. 2 in an Ornstein-Zernicke representation for the range of the lowest q vectors. The lines corresponds to the correlation lengths indicated. +, $\phi=6.4\times10^{-4}$ (sample 1) and △, $\phi=2.3\times10^{-3}$ (sample 2).

tion of the different correlation lengths showing up in the structure factor is difficult on the basis of the static measurements alone and will be facilitated by a comparison with the information about the aggregate dynamics.

B. Dynamics

On samples 2 ($\phi_{Pd}=2.3\times10^{-3}$) and 3 ($\phi_{Pd}=7.9\times10^{-3}$) an extensive series of x-ray photon correlation spectroscopy experiments were performed covering a q range from 1×10^{-3}Å^{-1} up to 8×10^{-3} Å^{-1}. As an example, a set of correlation functions is displayed in Fig. 5. From both samples a correlation function measured at a low q of 1.8×10^{-3} Å^{-1} and the correlation function measured at the highest q are presented. The curves measured are qualitatively similar to the previous data measured for the palladium aggregates in glycerol [14]. The time scale is shifted by

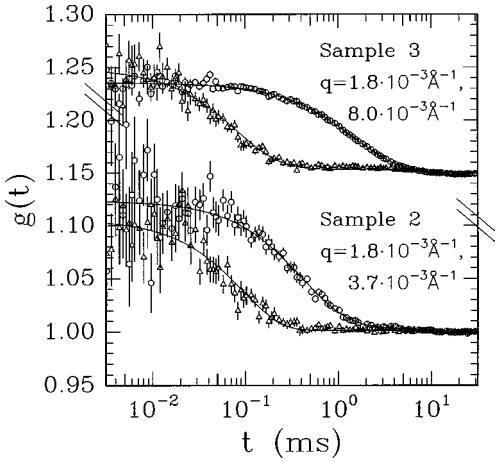

FIG. 5. Correlation functions $g(t)$ obtained at different concentrations and q values as indicated (lower curves, sample 2, $\phi=2.3\times10^{-3}$; upper curves, sample 3, $\phi=7.9\times10^{-3}$). The upper curves are shifted. Errors are estimated from photon counting statitistics. Lines are fits according to Eq. (24).

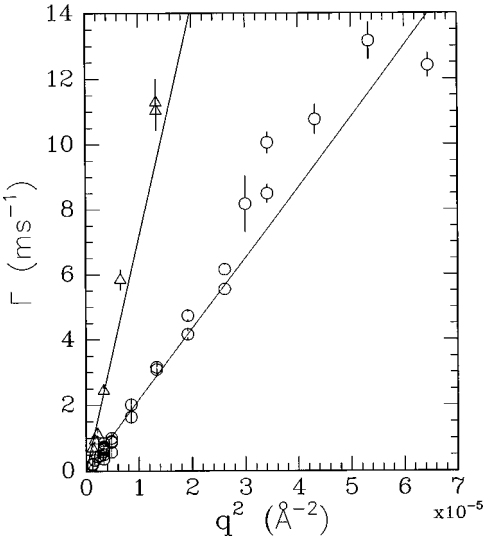

FIG. 6. Relaxation rate Γ versus q^2 for a suspension of Pd colloid at two concentrations: $\phi=2.3\times10^{-3}$, △ (sample 2) and $\phi=7.9\times10^{-3}$, ○ (sample 3). The slope corresponds to the diffusion coefficient measured.

about a factor of 1000 corresponding to the lower viscosity of water compared to glycerol.

The measured correlation functions (compare also Appendix B) can approximately be described by Eq. (20), but a better quantitative description of the whole curve can be obtained by using a cumulant expansion [19]. This expansion is used to describe a correlation function with a moderately broad distribution of relaxation rates as it is caused, e.g., by diffusion of a polydisperse collection of particles:

$$g(t)=1+A\,\exp\left[-(2\Gamma_q t)+\frac{\mu_2}{2}(2\Gamma_q t)^2-\frac{\mu_3}{6}(2\Gamma_q t)^3+-\cdots\right], \tag{24}$$

where 2Γ is the mean relaxation rate and μ_2 and μ_3 are the relative variance and skewness of the relaxation rate distribution, respectively. The lines in Fig. 5 show the model curves resulting from a fit with Eq. (24). The result of the analysis is displayed in Fig. 6, which shows the relaxation rate Γ as a function of q^2. The relative variance μ_2 is of the order of 20%, decreasing down to 10% at higher q values. The relaxation rate Γ is in both samples proportional to q^2. The slope of the line whose value gives the diffusion coefficient is largely different in the two samples. For sample 2 a diffusion coefficient $D=3.6\times10^{-12}$ m^2 s^{-1} results, corresponding to a hydrodynamic radius of $R_h=610$ Å $\pm10\%$($\eta_{H_2O}=10^{-3}$ Pa s). For sample 3 we get $D=1.1\times10^{-12}$ m^2 s^{-1}, showing that the diffusion is more than a factor of 3 slower.

VI. DISCUSSION

The analysis of the diffusive dynamics in terms of a hydrodynamic radius seems adequate for sample 2. At high q values the effective diffusion coefficient D approaches the self-diffusion coefficient D_s as discussed earlier. If hydrodynamic interactions are not too strong, a hydrodynamic radius

can at least be estimated from the measured value of D. There is an obvious agreement between the dominant correlation length in the structure factor and the value obtained for the hydrodynamic radius of the more dilute sample 2. If the shape of the measured $S(q)$ is interpreted in terms of the Guinier approximation (10) for a single aggregate, the correlation length ξ is related to the Guinier radius of the aggregates $R_{g,agg}=\sqrt{3}\xi=667$ Å$\pm 10\%$. This agrees well with the value obtained for the hydrodynamic radius ($R_h=610$ Å).

From this starting point a consistent picture emerges. The common length scale ξ visible in the structure factor at all concentrations measured corresponds to the typical size of the aggregates in the solution. Beyond $q\approx 2\times 10^{-3}$ the curves $I(q)$ are parallel, indicating that only the number but not the structure of the aggregates changes with concentration. At the lower concentration of sample 2 the translational diffusion of these aggregates dominates the dynamics. In this picture the additional longer correlation length showing up only at the lower concentrations (samples 1 and 2) is due to short-lived interaggregate correlation. A substantial fraction of very large aggregates otherwise would lead to a smaller diffusion coefficient.

At higher concentrations (sample 3) the aggregates start to overlap and the largest correlation length observable in this situation is of the order of the size of the individual aggregates, whose internal structure is still visible. We do not observe a peak in $S(q)$ in this situation and the dynamics of the sol is still liquidlike. In the q range under observation the correlation function still relaxes completely, i.e., no sign of gelation is observed. Nevertheless, the value of the diffusion coefficient decreases. Topological constraints due to overlap may to some extent be responsible for this slowing down, but there might also be a certain reduction of the viscosity due to the high surfactant content in the system.

We conclude that the general state of the system can be described as a sol of aggregates with a fractal internal structure. On a qualitative level the type of colloidal solution studied has some analogies to a polymer solution, for which the distinction between a dilute and a semidilute regime is made [29]. Above c^*, at which the size of the aggregates is comparable to their distance, they start to overlap. c^* roughly coincides with the highest concentration studied in this investigation.

The value of the fractal dimension is higher than observed in the well understood limits of diffusion and reaction limited growth kinetics [30–32], although similarly high values for d_f have been found in other systems [8]. It seems that the aggregates have undergone some process of restructuring, conceivably during the relatively complex process of production, which includes drying, dissolving, and precipitation [33]. Restructuring of fractal aggregates due to finite interaction energies was studied in simulations as well as in experiments [34,35]. As in our observation, the formation of more compact aggregates that did not lose their fractal properties completely were observed in that case.

Concerning the mechanism of stabilization, the data show that in the macroscopically stable colloidal solution not the individual particles but rather the aggregates as a whole are effectively stabilized by the surfactant. At present we can only offer a speculative explanation of this behavior. Obviously the particles cannot sustain a well defined stabilizing layer. It could be shown for flat surfaces that surfactants usually adsorb not as single molecules but as micellelike structures [36,37]. Conceivably the absorption process is hindered in the case studied here by the fact that the size of the particles is comparable to the size of the micelles. (SAXS experiments give a typical micelle radius of 2.6 nm.) An incomplete coverage by adsorbed micelles would lead to the formation of mixed particle-micelle aggregates and aggregates covered by micelles. The question to what extent the mentioned restructuring of the aggregate takes place directly during the synthesis or later on cannot yet be answered.

VII. SUMMARY

We have studied the structural and dynamic features of a colloidal solution consisting of surfactant-stabilized aggregates at several concentrations up to the semidilute state. We have shown that the solutions under study consist microscopically of fractal aggregates with a typical radius of about 600 Å. The analysis of the structure factor and of the dynamic behavior led to consistent results. Structural changes induced by changing the concentration can be attributed to interaggregate correlation in a system of partially overlapping aggregates. At all concentrations the basic structural features of the individual aggregates can be seen in the structure factor. Whereas at lower concentrations the time scale of the dynamics is dominated by the translational diffusion of the single aggregates, we observed a slowing down at the higher concentration. The data indicate that constraints due to overlap between the aggregates are at least partially at the origin of this behavior. Gelation and structure formation leading to a peak in the intensity $I(q)$ was not observed. In all cases the system can be described as a sol of aggregates.

We hope to have demonstrated in this study some of the promising possibilities the technique of XPCS offers, namely, the study of the dynamics of concentrated and structured systems in a q range corresponding to the structurally relevant length scale.

ACKNOWLEDGMENTS

We are very grateful to E. W. Fischer and B. Ewen for their reliable support of this project. We thank Henri Gleyzolle and Patrick Feder for technical assistance and H. Ladinski for his help during the experiment. Financial support by the Bundesministerium für Bildung und Forschung (BMBF Contract No. ME11.07K) and the Deutsche Forschungsgemeinschaft (SFB 262) is gratefully acknowledged.

APPENDIX A: STATISTICAL ERROR OF THE CORRELATION FUNCTION

At low count rates the error due to Poisson counting statistics is the dominant contribution to the statistical error of the correlation function [38]

$$\Delta g(t)=\sqrt{g(t)}\frac{1}{\langle I\rangle\sqrt{T\Delta t}}. \tag{A1}$$

In this expression I is the count rate, T the total counting time, and Δt the sampling interval. Since Δt decreases with

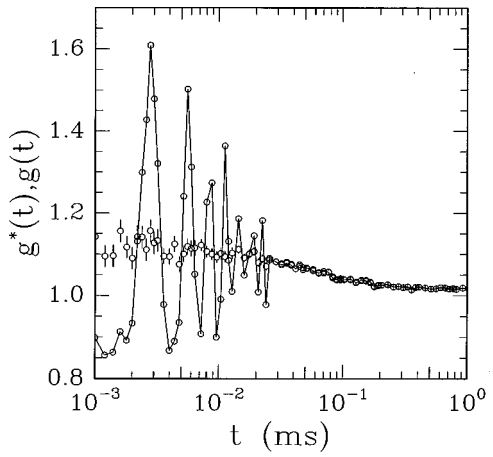

FIG. 7. Correlation function $g(t)$ before and after division by a correlation function $g_{synchr}(t)$ measured on the primary beam. The oscillations correspond to the 2/3-filling mode of the ESRF and are removed by the division.

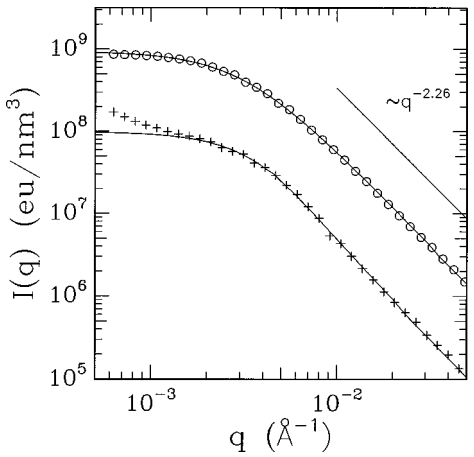

FIG. 8. Scattering cross section $I(q)$ vs q of a Pd colloid from sample 1 ($\phi=6.4\times10^{-4}$, +) and sample 3 ($\phi=7.9\times10^{-3}$, ○). The solid lines show fits of the model functions (C1) and (13). The additional increase of $I(q)$ at the lowest q is disregarded. The data obtained from sample 1 decay more steeply, giving rise to a sigmoidal shape of $S(q)$.

the argument t of the correlation function $g(t)$, the statistical error increases at short times. This error at short times in comparison to the value of the intercept of $g(t)$ defines the largest measurable relaxation rate and therefore the high q limit. In our experiment the intercept of $g(t)$ takes values around 0.1. Based on a statistical analysis of a static speckle pattern, this value could be understood as a consequence of incoherent contributions in the primary beam [23].

APPENDIX B: PRIMARY BEAM CONTRIBUTION TO THE CORRELATION FUNCTION

A complication while performing XPCS measurements covering the time range below milliseconds arises from the fact that the x-ray beam from a synchrotron radiation source is usually strongly modulated due to the nonhomogeneous filling of the synchrotron. Since the resulting oscillations in the primary beam intensity are not correlated with the fluctuations caused by the dynamics of the sample, the resulting correlation function $g^*(t)$ is the product of the two contributions

$$g^*(t)=g_{synchr}(t)g_{sample}(t). \tag{B1}$$

For a multiple sampling time correlator, as used in this experiment, the sampling interval Δt increases with increasing argument t of the correlation function. The correlation function measured is described by the following expression, which leads to an effective damping of the oscillation caused by the primary beam fluctuations [38]:

$$g_{\Delta t}(t)=\frac{1}{\Delta t^2}\int_{-\Delta t/2}^{\Delta t/2}(\Delta t-|t'|)g^*(t+t')dt'. \tag{B2}$$

If the time constants of both components $g_{synchr}(t)$ and $g_{sample}(t)$ are well separated, one component is always approximately constant within the integration interval and can be taken out of the integral. It is then easy to remove the influence of the primary beam oscillations from the measured correlation function. $g_{synchr}(t)$ is measured separately on the primary beam directly and $g(t)=g^*(t)/g_{synchr}(t)$ can be calculated channel by channel. This procedure is used for the data presented in this article and is illustrated in Fig. 7. The observed oscillations correspond to the 2/3-filling mode of the ESRF, with the period of 2.81 μs reflecting the time a relativistic electron needs to travel along the storage ring circumference of 845 m. The correction allows a much broader time range to be used for determining the intercept of the correlation function.

APPENDIX C: INFLUENCE OF THE CUTOFF FUNCTION ON THE AGGREGATE STRUCTURE FACTOR

There is a subtle change in the exact shape of the structure factor at different concentrations for the samples studied. A closer inspection of the data reveals that $S(q)$ in between the Guinier and the fractal range decays more steeply at lower concentration, in a way that cannot satisfactorily be described by expression (13). A similar shape was observed for structure factors calculated from simulated aggregates [39] and it was attributed to the exact outer shape of the aggregates. We found indeed that our data can be described by a sharper cutoff, which can be realized in the model used by introducing an exponent $\gamma>1$ in the exponential cutoff function used before. As suggested in [40], one may take

$$S(q)\propto\int r^{d_f-3}\exp[-(r/\xi)^{\gamma}]\frac{\sin(qr)}{qr}r^2dr. \tag{C1}$$

Figure 8 shows a detailed view of $I(q)$ in the relevant q range including a fit of the model function (C1) to the data obtained from sample 1. In this case γ takes a value of 1.5. The additional increase in $I(q)$ at the lowest q is disregarded here. The model describes the data very well in the q range, which reflects the structure of the individual aggregates. Data and a model function for sample 3 are included in the figure for a better comparison. The fact that the sharper cutoff is observable at low concentration is another indication of the existence of overlap occurring in the more concentrated samples.

[1] T. A. Witten and L. M. Sander, Phys. Rev. Lett. **47**, 1400 (1981).
[2] M. Muthukumar, Phys. Rev. Lett. **50**, 839 (1983).
[3] P. Meakin, Phys. Rev. Lett. **51**, 1119 (1983).
[4] M. Kolb, R. Botet, and R. Jullien, Phys. Rev. Lett. **51**, 1123 (1983).
[5] R. Jullien, M. Kolb, and R. Botet, J. Phys. (France) Lett. **45**, 211 (1984).
[6] D. A. Weitz and M. Oliveria, Phys. Rev. Lett. **52**, 1433 (1984).
[7] D. W. Schaefer, J. E. Martin, P. Wiltzius, and D. S. Cannell, Phys. Rev. Lett. **52**, 2371 (1984).
[8] T. Freltoft, J. K. Kiems, and S. K. Sinha, Phys. Rev. B **33**, 269 (1986).
[9] M. Carpineti and M. Giglio, Phys. Rev. Lett. **68**, 3327 (1992).
[10] M. Carpineti and M. Giglio, Phys. Rev. Lett. **70**, 3828 (1993).
[11] M. D. Haw, M. Sievwright, W. C. K. Poon, and P. N. Pusey, Physica A **217**, 231 (1995).
[12] A. H. Krall, Z. Huang, and D. A. Weitz, Physica A **235**, 19 (1997).
[13] S. B. Dierker, R. Pindak, R. M. Fleming, I. K. Robinson, and L. E. Berman, Phys. Rev. Lett. **75**, 449 (1995).
[14] T. Thurn-Albrecht, W. Steffen, A. Patkowski, G. Meier, E. W. Fischer, G. Grübel, and D. L. Abernathy, Phys. Rev. Lett. **77**, 5437 (1996).
[15] G. Porod, in *Small Angle X-Ray Scattering*, edited by O. Glatter and O. Kratky (Academic, London, 1982).
[16] I. S. Gradshteyn and I. M. Ryzhik, *Tables of Integrals, Series and Products* (Academic, Orlando, 1980), p. 707.
[17] R. Vacher, T. Woignier, and J. Pelous, Phys. Rev. B **37**, 6500 (1988).
[18] B. Berne and R. Pecora, *Dynamic Light Scattering* (Wiley-Interscience, New York, 1975).
[19] B. Chu, *Laser Light Scattering* (Academic, San Diego, 1991).
[20] P. N. Pusey, in *Liquids, Freezing and Glass Transition*, 1991 Les Houches Lectures, edited by J. P. Hansen, D. Levesque, and J. Zinn-Justin (North-Holland, Amsterdam, 1991).
[21] O. Diat, P. Bösecke, J. Lambard, and P. P. E. A. De Moor, J. Appl. Crystallogr. **30**, 862 (1997).
[22] G. R. Strobl, Acta Crystallogr., Sect. A: Cryst. Phys., Diffr., Theor. Gen. Crystallogr. **26**, 367 (1970).
[23] D. L. Abernathy, G. Grübel, S. Brauer, I. McNulty, G. B. Stephenson, S. G. J. Mochrie, A. R. Sandy, N. Mulders, and M. Sutton, J. Synchrotron Radiat. **5**, 37 (1998).
[24] M. T. Reetz and W. Helbig, J. Am. Chem. Soc. **116**, 7401 (1994).
[25] M. T. Reetz and S. A. Quaiser, Angew. Chem. **107**, 2461 (1995); Angew. Chem. Int. Ed. Engl. **34**, 2240 (1995).
[26] M. G. Koch (unpublished).
[27] M. Winter, Ph.D. thesis, Ruhr-Universität Bochum, 1998 (unpublished).
[28] J. G. Weers, J. F. Rathman, F. U. Axe, C. A. Chrichlow, L. D. Foland, D. R. Scheuing, R. J. Wiersema, and A. G. Zielske, Langmuir **7**, 854 (1991).
[29] P. G. de Gennes, *Scaling Concepts in Polymer Physics* (Cornell University Press, Ithaca, 1979).
[30] D. A. Weitz, J. S. Huang, M. Y. Lin, and J. Sung, Phys. Rev. Lett. **54**, 1416 (1985).
[31] D. A. Weitz and M. Y. Lin, Phys. Rev. Lett. **57**, 2037 (1986).
[32] P. Dimon, S. K. Sinha, D. A. Weitz, C. R. Safinya, G. Smith, W. A. Varady, and H. Lindsay, Phys. Rev. Lett. **57**, 595 (1986).
[33] S. A. Quaiser, Ph.D. thesis, Philips-Universität Marburg, 1995 (unpublished).
[34] W.Y. Shih, J. Liu, W. H. Shih, and I. Aksay, J. Stat. Phys. **62**, 961 (1991).
[35] M. D. Haw, M. Sievwright, W. C. K. Poon, and P. N. Pusey, Adv. Colloid Interface Sci. **62**, 1 (1995).
[36] S. Manne and H. E. Gaub, Science **270**, 1480 (1995).
[37] M. Jaschke, H.-J. Butt, H. E. Gaub, and S. Manne, Langmuir **13**, 1381 (1997).
[38] K. Schätzel, in *Dynamic Light Scattering*, edited by W. Brown (Clarendon, Oxford, 1993).
[39] R. Thouy and R. Jullien, J. Phys. I **6**, 1365 (1996).
[40] T. Nicolai, D. Durand, and J.-C. Gimel, Phys. Rev. B **50**, 16 357 (1994).